Creating long term gridded fields of reference evapotranspiration in Alpine terrain based on a re-calibrated Hargreaves method

K. Haslinger[1], A. Bartsch[1]

[1]{Central Institute for Meteorology and Geodynamics (ZAMG), Climate Research Department, Vienna, Austria}

Correspondence to: K. Haslinger (klaus.haslinger@zamg.ac.at)

Abstract

A new approach for the construction of high resolution gridded fields of reference evapotranspiration for the Austrian domain on a daily time step is presented. Gridded data of minimum and maximum temperatures are used to estimate reference evapotranspiration based on the formulation of Hargreaves. The calibration constant in the Hargreaves equation is recalibrated to the Penman-Monteith equation in a monthly and station-wise assessment. This ensures on one hand eliminated biases of the Hargreaves approach compared to the formulation of Penman-Monteith and on the other hand also reduced root mean square errors and relative errors on a daily time scale. The resulting new calibration parameters are interpolated in time to a daily temporal resolution for a standard year of 365 days. The overall novelty of the approach is the use of surface elevation as the sole predictor to estimate the re-calibrated Hargreaves parameter in space. A third order polynomial is fitted to the re-calibrated parameters against elevation at every station which yields the statistical model for assessing these new parameters in space by using the underlying digital elevation model of the temperature fields. Having newly calibrated parameters for every day of year and every grid point, the Hargreaves method is applied to the temperature fields, yielding reference evapotranspiration for the entire grid and time period from 1961-2013. With this approach it is possible to generate high resolution reference evapotranspiration fields starting when only temperature observations are available but re-calibrated to meet the requirements of the recommendations defined by the Food and Agricultural Organisation (FAO).

1 Introduction

The water balance in its most general form is determined by the fluxes of precipitation, change in storage and evapotranspiration (Shelton 2009). Particularly for the latter, measurement is rather costly, since it requires sophisticated techniques like eddy correlation methods or lysimeters. In hydrology as well as agriculture the actual evapotranspiration as part of the water balance equation is mostly assessed from the potential evapotranspiration (PET). PET refers to the maximum moisture loss from the surface, determined by meteorological conditions and the surface type, assuming unlimited moisture supply (Lhomme 1997). Since surface conditions determine the amount of PET, the concept of reference evapotranspiration (ET0) was introduced (Doorenbos and Pruitt, 1977). ET0 refers to the evapotranspiration from a standardized vegetated surface (grass) under unrestricted water supply, making ET0 independent of soil properties. Numerous methods exist for estimating ET0; differences arise in the complexity and the amount of necessary input data for calculation.

A standard method, recommended by the Food and Agricultural Organisation (FAO; Allen et al. 1998), is the Penman-Monteith (PM) formulation of ET0. There are of course countless other methods as thoroughly described in McMahon et al. (2013), but the PM equation is considered the most reliable estimate and serves as a standard for comparisons with other methods (Allen et al. 1998). PM is fully physically based and requires four meteorological parameters (air temperature, wind speed, relative humidity and net radiation). It utilizes energy balance calculations at the surface to derive ET0 and is therefore considered a radiation based method (Xu and Singh 2000).

On the contrary, much simpler methods which use air temperature as a proxy for radiation (Xu and Singh 2001) have been developed to overcome the shortcoming of PM of not having sufficient input data. In this paper, the method of Hargreaves (HM, Hargreaves et al. 1985) is used. It requires minimum and maximum air temperature and extra-terrestrial radiation, which can be derived by the geographical location and the day of year. Though much easier to calculate, as temperature observations are dense and easily accessible, one has to be aware that the HM, among most temperature based estimates, are developed for distinct studies and/or regions, representing a rather distinct climatic setting (Xu and Singh, 2001). To avoid large errors, these methods need to undergo a recalibration procedure to make them applicable to different climatic regions than they were originally designed for (Chattopadhyay and Hulme 1997, Xu and Chen 2005).

In this paper the method for constructing a dataset of ET0 on a daily time resolution and a 1 km spatial resolution based on the method of Hargreaves is presented. The HM is calibrated to the PM on a station-wise assessment. Many studies describe re-calibration procedures for ET0 estimations in general (Tegos et al., 2015; Oudin et al. 2005) and for the HM in particular (Pandey et al. 2014; Tabari and Talaee, 2011; Bautista et al., 2009; Gavilán et al. 2006) in order to achieve similar results compared to PM. There are also some studies describing methods for creating interpolated ET0 estimates (e. g. Aguila and Polo, 2011; Todorovic et al, 2013). However, two main methodological frameworks emerged for the interpolation of ET0 (McVicar et al., 2007): (i) interpolation of the forcing data and then calculating ET0, or (ii) calculating ET0 at every weather station and the interpolating ET0 onto the grid. In this paper we follow the first approach and combine it with methods proposed by Tegos et al. (2015) and Mancosu et al. (2014) which use spatially interpolated ET0 model parameters. Gridded data of minimum and maximum temperatures are used as forcing fields for the application of the Hargreaves formulation of ET0. The novelty of this study is the application of elevation as a predictor for the interpolation of the re-calibrated HM calibration parameter. Furthermore, these new calibration parameters are also variable in time, by changing day-by-day for all days of the year. This approach goes a step further than the method of Aguilar and Polo (2011) which derived one new calibration parameter for the dry and one for the wet season of the year.

The presented dataset aims to use the better of two worlds by (i) using a method for estimating ET0 that is calibrated to the standard algorithm as defined by the FAO and (ii) being applicable to a comprehensive, long-term forcing dataset and on a high temporal and spatial resolution.

2 Forcing Data

The foundation of the ET0 calculations is a high resolution gridded dataset of daily minimum and maximum temperatures calculated for the Austrian domain (SPARTACUS, see Hiebl and Frei 2015), whereas the actual data stretches beyond Austria to entirely cover catchments close to the border. SPARTACUS is an operationally, daily updated dataset starting in 1961 and reaching down to the present day. For the conduction of the ET0 fields, the SPARTACUS temperature forcing is used for the period 1961-2013. The interpolation algorithm is tailored for complex, mountainous terrain with spatially complex temperature distributions. SPARTACUS also aims to ensure temporal consistency through a fixed station network over the whole time period, providing robust trend estimations in space. SPARTACUS uses the SRTM (Shuttle Radar Topography Mission, Farr and Kobrick 2000) version 2 Digital Elevation Model (DEM), so the SRTM DEM is also applied in the present study.

SPARTACUS provides the input data for calculating ET0 following the Hargreaves method (HM, Hargreaves and Samani 1982, Hargreaves and Allen 2003). However, a recalibration of the HM is necessary to avoid considerable estimation errors. This is carried out in a station wise assessment. Data of 42 meteorological stations (provided by the Austrian Weather Service ZAMG) is used to monthly calibrate the HM to the Penman-Monteith Method (PM). Figure 1 shows the location of these stations, which are spread homogeneously among the Austrian domain and also comprise rather different elevations and environmental settings (Table 1). Data of daily global radiation, wind speed, humidity, maximum and minimum temperatures covering the period 2004-2013 are used to calculate ET0 simultaneously with HM and PM.

3 Methods

3.1 Estimating reference evapotranspiration

As explained above, numerous methods exist for the estimation of ET0, which is defined as the maximum moisture loss from a standardized, vegetated surface, determined by the meteorological forcing (Shelton, 2009). They can roughly be classified as temperature based and radiation based estimates (Xu and Singh, 2000, Xu and Singh, 2001, Bormann, 2011). Following the recommendations of the FAO (Allen et al. 1998) the radiation-based Penman-Monteith Method (PM) provides most realistic results and generally outperforms temperature based methods. The overall shortcoming of the PM is the data intense calculation algorithm which requires daily values of net radiation, wind speed, humidity, maximum and minimum temperatures. Data coverage for these variables is usually rather sparse, particularly if gridded data is required. ET0 following the PM is calculated as displayed in Equation 1:

$$ET0\_p = \frac{0.408\Delta(R_N - G) + \gamma \frac{900}{T+273} u_2 (e_s - e_a)}{\Delta + \gamma(1 + 0.34 u_2)} \quad (1)$$

where E is the reference evapotranspiration [mm day^{-1}], R_N is the net radiation at the crop surface [MJ m^{-2} day^{-1}], G is the soil heat flux density [MJ m^{-2} day^{-1}], T is the mean air temperature at 2 m height [°C], u_2 is the wind speed at 2 m height [m s^{-1}], e_s is the saturation vapour pressure [kPa], e_a is the actual vapour pressure [kPa]; giving the vapour pressure deficit by subtracting e_a from e_s; Δ is the slope of the vapour pressure curve [kPa °C^{-1}] and γ is the psychrometric constant [kPa °C^{-1}]. Given the time resolution of one day the soil heat flux term is set to zero. The calculation of the other individual terms of Equation 1 is described in Allen et al. (1998). It should be mentioned, that the original Penman-Monteith equation contains a “surface resistance” term, expressing the response of different vegetation types, which is set constant for FAO PM, since it uses a standardized vegetated surface.

In contrast to the radiation based PM, the HM is based on daily minimum and maximum temperatures (T_{min}, T_{max}). Hargreaves (1975) stated from regression analysis between meteorological variables and measured ET0 that temperature multiplied by surface global radiation is able to explain 94 % of the variance of ET0 for a five day period (see Hargreaves and Allen 2003). Furthermore, wind and relative humidity explained only 10 and 9 % respectively. Additional investigations by Hargreaves led to an assessment of surface radiation which can be explained by extra-terrestrial radiation at the top of the atmosphere and the diurnal temperature range as an indicator for the percentage of possible sunshine hours. The final form of the Hargreaves equation is given by:

$$ET0\_h = C(T_{mean} + 17.78)(T_{\max} - T_{\min})^{0.5} R_a \quad (2)$$

where ET0_h is the reference evapotranspiration [mm day^{-1}], T_{mean}, T_{max} and T_{min} are the daily mean, maximum and minimum air temperatures [°C] respectively and R_a is the water equivalent of the extra-terrestrial radiation at the top of the atmosphere [mm day^{-1}]. C is the calibration parameter of the HM and was set to 0.0023 in the original Hargreaves et al. (1985) publication.

Following these formulations the ET0 for all stations was calculated for the period 2004-2013. Figure 2a shows, as an example, the daily time series of ET0 as derived by PM (ET0_p) and HM (ET0_h) in the year 2004 at the station Grossenzersdorf. The differences between those two are obvious as ET0_p shows clearly higher variability, with ET0_h underestimating the upward peaks in the cold season and downward peaks in the warm season. This feature is more noticeable in Figure 2b, which shows the monthly averages over all stations, indicating the spread among all 42 stations. Here, an underestimation of the ET0_h compared to ET0_p from October to April is counteracted by an overestimation between May and September. On the other hand, ET0_h shows higher spread among stations compared to ET0_p except for November to January.

These features are also reflected in the bias of ET0_h compared to ET0_p as can be seen in Figure 3a. The average monthly bias over all stations is negative in the cold season with largest deviations in February of 0.3 mm day^{-1}, compared to the peak average positive bias in June of 0.4 mm day^{-1}. The annual cycle of the Root Mean Squared Error (RMSE) of ET0_h as displayed in Figure 3b shows peak values in summer mainly due to the higher absolute values in the warm season compared to wintertime. The RMSE in December is around 0.5 mm day^{-1} compared to 1.1 mm day^{-1} in July, showing some more spread in wintertime compared to summer.

3.2 Calibration

In order to achieve a meaningful representation of ET0 by HM, an adjustment of the calibration parameter (C_{adj}) of HM is necessary, with respect to ET0 derived from PM. This is carried out on an average monthly basis for every station by the following equation, as also proposed by Bautista et al. (2009):

$$C_{adj} = 0.0023/(E_H / E_P) \qquad (3)$$

where C_{adj} represents the new calibration parameter of the HM, E_H is the original ET0_h from HM, using a C of 0.0023 and E_P is the ET0_p from PM. As a result, a new set of C values for every month and every station is available.

Figure 4 shows the adjusted C values for three exemplary stations. C_{adj} is generally higher in winter and autumn compared to the original value indicated by the dashed line at 0.0023. It is also obvious that at station Grossenzersdorf the original value is matching rather well to the C_{adj} from April to October, in the other months the adjusted values are clearly higher. On the contrary, at station Weissensee_Gatschach C_{adj} is lower than 0.0023 except for the months from November to February. At station Rudolfshuette-Alpinzentrum the adjusted values are above the original ones all time of the year, reaching rather high values in wintertime of about

0.007. These results clearly underpin the necessity for a re-calibration of C in order to receive sound ET0 from temperature.

After determining the values for C_{adj} the ET0 was re-calculated with these new calibration parameter values (ET0_h.c). For simplicity for this first assessment the monthly values of C_{adj} were used for all days of the month, no temporal interpolation was conducted. As a result, the monthly mean bias, as was shown in Figure 4a, is reduced to zero at every station. Furthermore, the RMSE has also slightly decreased by 0.1 to 0.2 mm day^{-1}, as can be seen in Figure 5a. The Relative Error (RE) has also decreased, from around 50 % to fewer than 40 % in January for example (cf. Figure 5b). The improvements regarding RE in summer are lower due to the higher absolute values of ET0 in the warm season.

The complete monthly mean time series from 2004 to 2013 of ET0_p, ET0_h and ET0_h.c for three stations are shown in Figure 6. At station Grossenzersdorf the underestimation of ET0_h in winter is reduced as well as the overall underestimation at station Rudolfshuette-Alpinzentrum. On the other hand, the overestimation in summer at station Weissensee-Gatschach is considerably reduced with ET0_h.c. These features in combination with the information on the altitude of the given stations provide some information on more general characteristics of C_{adj} and the effects of the calibration. It seems that there is an altitude-dependence of C_{adj}, which is displayed in more detail in Figure 7. It shows the monthly average C_{adj} for stations which where binned to distinct classes of altitude ranging from 100 to 2300 m in steps of 100 m. As already seen in Figure 4 as an example for three stations, C_{adj} is clearly higher in winter than the unadjusted value. From April to September C_{adj} is lower than 0.0023 up to altitudes of 1500 m.a.s.l., lowest values are visible in May to August between altitudes of 400 to 1000 m.a.s.l.

3.3 Temporal and spatial interpolation of the Hargreaves calibration parameter C_{adj}

The monthly adjusted calibration parameters are now interpolated in space and time in order to receive a congruent overlay of C_{adj} over the SPARTACUS grid for every day of year. As a first step, the monthly C_{adj} values at every station are linearly interpolated to daily values to avoid stepwise changes and therefore abrupt shifts of C_{adj} between months. This is carried out for a standard year with length of 365 days. The result is a time series of daily changing values of C_{adj} over the course of the year, available for every station, stretching over different altitudes and therefore yielding 42 different annual time series of C_{adj}.

Subsequently the daily, station-wise values of C_{adj} are interpolated in space. As was shown in the previous section, C_{adj} changes with altitude. Figure 8 shows the adjusted calibration parameters plotted against altitude for the monthly means of C_{adj}. From this Figure it comes clear that this relationship is not linear. C_{adj} is decreasing from the very low situated stations until altitudes between 500 and 1000 m.a.s.l. Going further up C_{adj} increases and one could say it might be a linear increase, particularly in winter. On the other hand, looking at the summer months the station with the highest elevation (Sonnblick, 3106 m.a.s.l.) shows somewhat lower or at least equal values of C_{adj} compared to the cluster of stations between 2000 and 2400 m.a.sl. This feature indicates that the relationship above 1000 m.a.s.l. might not be linear. Taking all this characteristics into account, a higher order polynomial fit was chosen to describe the C_{adj}-altitude relation. As shown in Figure 8 a third order polynomial fit, indicated by the red line, is applied. Using the underlying DEM of the SPARTACUS dataset it is possible to determine adjusted calibration parameters for every grid point in space by this relationship. The polynomial fit is applied for every day of the daily interpolated station-wise C_{adj} values, since these are changing day by day as well. The result is a gridded dataset of C_{adj} for the SPARTACUS domain for 365 time steps from January 1st to December 31st. Figure 9 shows two examples of C_{adj} distribution in space on January 1st (a) and July 1st (b). Particularly in January the altitude dependence of the calibration parameter is clearly standing out, showing rather high values of C_{adj} in the mountainous areas. In contrast to winter the spatial variations in summer are smaller, only some central Alpine areas between 1000 and 3000 m.a.s.l. are appearing in somewhat different shading than the surrounding low lands.

Having these gridded C_{adj} values the ET0_h.c is calculated for every grid point and day since 1961 to 2013. In the case of leap years the C_{adj} grid of February 28th is also used for February 29th.

4 Results

Figure 10a shows the climatological mean (1961-2013) of the daily ET0 fields over the whole domain. Lowest daily mean values of below 1.5 mm day^{-1} are apparent on the highest mountain ridges of the main Alpine crest. Highest values of 2.4 mm day^{-1} and above are found in the eastern and southern low lands. Other spatial features are visible as well, for example the higher ET0 in the valleys in the far western part of Austria. It is driven by the higher sunshine hours in these areas, which are also termed as “inner alpine dry valleys”, because rainfall approaching from the west is often screened by the mountain chains in the Northwest. In the ET0 estimate it is reflected in the higher Diurnal Temperature Range (DTR), yielding larger values in that particular area. A similar characteristic is apparent in the very south of Austria. Here the ET0 is higher as well, compared to topographically similar regions on the northern rim of the Alps. This is again connected to the higher proportion of sunshine hours which enhances indirectly ET0 through higher DTR values.

Figure 10b shows exemplary the ET0 field of August 8th 2013. For the first time on that particular day, temperatures reached above 40 °C in Austria at some stations in the East and South. Values of ET0 are particularly high, reaching up to 7 mm day^{-1} in some areas in the Southeast. That day was also characterized by an approaching cold front, bringing rain, dropping temperatures and overcast conditions from the West. This is featured as well in the ET0 field, showing a considerable gradient from West to East, with nearly zero ET0 at the headwaters of the Inn River in the far Southwest of the domain. Furthermore, the implications of overcast conditions in the West with lower altitudinal gradients of ET0 compared to the East with sunny conditions and distinct gradients along elevation are visible.

July, the month with the highest absolute values of ET0 shows considerable variations in the last 53 years. As an example, the mean anomaly of ET0 in July of 1983 with respect to the July mean of 1961-2013 is displayed in Figure 11a. This month was characterized by a considerable heat wave and mean temperature anomalies of +3.5 °C which also affected ET0. The absolute anomaly of ET0 reaches above 1 mm day^{-1} with respect to the climatological mean in some areas. The relative anomaly is in a range between 10 to 30 % (Figure 11c). On the other hand, July of 1979 was rather cool with temperatures 1.5 °C below the climatological mean and accompanied by a strong negative anomaly in sunshine duration, particularly in the areas north of the main Alpine crest. These characteristics implicated a distinctly negative anomaly of ET0 in this particular month (Figure 11b). The absolute anomaly stretches between 0 and more than -1 mm day^{-1}, equivalent to a relative anomaly of 0 to -30 % (Figure 11d). The negative signal is stronger in the areas north of the Alpine crest, zero anomalies are found in the some areas south of the main Alpine crest.

In Figure 12 the overall benefits of the re-calibration of the HM are revealed. It shows the mean ET0 in July 2012, a month accompanied by a considerable heat wave at the beginning and an overall temperature anomaly of around +2 °C. In Figure 12b the ET0 field of the original HM formulation without calibration is shown, and Figure 12a displays the results with re-calibration as described in this study. Overall, the gradient along elevation of ET0 is larger in the non-calibrated field. Particularly in this time of the year with large absolute values, the re-calibration has a considerable impact, although C_{adj} in July is relatively small compared to winter. As shown before (cf. Figure 4), the ET0 estimation using the original C is good for July in the lowlands, since biases tend to be rather small. However, going to higher elevations, the overestimation of the original HM is rather pronounced. Mean biases reach +1 mm day^{-1} or +30 %. This signal switches to negative biases of -0.5 mm day^{-1} (-25 %) above 1500 m.a.s.l.

5 Discussion

By comparing the characteristics of ET0 based on HM and PM on a daily time step it came clear that a re-calibration of C within the formulation of Hargreaves follows distinct patterns. The values of C_{adj} show markedly variations in space and time (over the course of the year). It turned out, that a monthly re-calibration of C reveals an annual cycle of C_{adj}, with C_{adj} being close to the original value of 0.0023 in the warm season (April-October) and low elevations. Going to higher elevations, C_{adj} decreases until roughly 1000 m.a.s.l. Reaching altitudes above 1700 m.a.s.l., C_{adj} is generally above the original 0.0023, particularly in the cold season (November-March). This altitude dependency of the calibration parameter in HM is mentioned in Samani (2000), but the authors also claimed that this relationship may be affected by different latitudes. Aguila and Polo (2011) also found that the original HM using a C of 0.0023 underestimates ET0 at higher elevations and defined a value of 0.0038 at an elevation of 2500 m.a.s.l. However, this altitude dependency of C turned out to be more complex, as we are able to display, showing a distinct variation throughout the year along with elevation. So this relationship is used to derive C_{adj} values for every day of year and every grid point of the forcing fields.

To reveal the sources of this altitude dependence of C we accomplished some additional analysis. In general, the HM utilizes the Diurnal Temperature Range (DTR, T_{max} minus T_{min}) to mimic the amount of global radiation at the land surface. Clear sky conditions are usually associated with higher DTR. There will be more heating during daytime due to large proportions of direct solar radiation, whereas at night time temperatures are dropping further down since the outgoing long-wave radiation is not reflected by clouds. The connection between DTR and radiation is shown in numerous studies (Pan et al., 2013; Makowski et al., 2009; Bindi and Miglietta, 1991; Bristow and Campbell, 1984). All these investigations showed considerable correlations, for example Makowski et al. 2009 reported a correlation coefficient of 0.87 of the annual means of DTR and solar radiation averaged over 31 stations across Europe.

Figure 13 shows the correlation of DTR and global radiation on a daily time scale at the 42 stations used in this study. The coefficients show a distinct altitudinal dependency, particularly in winter. In January the correlations are above 0.90 at some stations and generally high at altitudes between 400 and 1000 m.a.s.l. At higher elevations the correlations are dropping considerably, getting negative between 1500 and 2000 m.a.s.l. In July the correlations are generally higher. Apart from two stations the correlations lie between 0.45 and 0.98, but again accompanied by a decline with altitude, which is also seen in the year round correlations. Interestingly, the patterns of the correlations along altitude are rather similar to the C_{adj} patterns as can be seen in Figure 8. Therefore we think that the DTR-global radiation nexus is the crucial point in the altitude dependence of C_{adj}.

The reasons for the correlation patterns in Figure 13 seem to be rooted in the lower atmospheric mixing ratios at the lowest stations, some of them located in, or nearby cities, which might dampen the DTR, although clear sky conditions are apparent. At moderate altitudes between 400 and 1500 m.a.s.l. the daily temperature amplitude is more dominantly driven by surface energy balance processes which reflects the higher correlations. Going further up, the proportion of the DTR which is determined by large scale air mass changes rises, as the station locations reach up above the planetary boundary layer into the free atmosphere, causing considerably low correlations at higher elevations, particularly in winter.

Although these circumstances seem to be a drawback of the methodology, the overall effect is only minor. Figure 14 shows the HM ET0 in dependence of the DTR and the daily mean temperature. At low daily mean temperatures, between -10 and +10 °C, the contour lines determining the value of ET0 are rather steep. This implies that a change in DTR has only minor effects on the ET0 outcome, whereas a change in daily mean temperature is more important.

However, the procedure of altering C has also implications on the variability of ET0 on a daily time scale. As was visible in Figure 2a the variability of ET0 based on HM is lower than using PM. The presented re-calibration has only little effect on the enhancement of variability. By scaling C, variability is slightly enhanced in those areas and time of the year where C_{adj} is higher than 0.0023. This is the case for most of the time and widespread areas, but there are regions or altitudinal levels where the opposite is taking place. As is visible in Figure 8 areas up to 1500 m.a.s.l. show lower than original values of C_{adj} in the summer months. There are particular areas in June between altitudes of 500 to 1000 m.a.s.l. that show the largest deviation from the original value. In these areas variability is lower in the re-calibrated version. On the other hand the benefit of an ET0 formulation being unbiased compared to the reference of PM may overcome these shortcomings.

The overall performance of the final gridded dataset compared to the PM estimates is displayed in Figure 15. 15a shows the monthly bias of the original HM ET0 and the calibrated ET0 of the nearest grid point. The bias is clearly reduced in nearly all months. However, in April, as the only exception, the bias of the calibrated grid point values is larger than the bias of the original estimation. The biases concerning different levels of altitude are reduced as well, as can be seen in Figure 15b which shows the biases in July and Figure 15c displaying the biases in January.

6 Conclusion

In this paper a gridded dataset of ET0 for the Austrian domain from 1961-2013 on daily time step is presented. The forcing fields for estimating ET0 are daily minimum and maximum temperatures from the SPARTACUS dataset (Hiebl and Frei 2015). These fields are used to calculate ET0 by the formulation of Hargreaves et al. (1985). The HM is calibrated to the Penman-Monteith equation, which is the recommended method by the FAO (Allen et al. 1998), at a set of 42 meteorological stations from 2004-2013, which have full data availability for calculating ET0 by PM. The adjusted monthly calibration parameters C_{adj} are interpolated in time (resulting in daily C_{adj} for a standard year) and space (resulting in C_{adj} for every grid point of SPARTACUS and day of year). With these gridded C_{adj} the daily fields of reference evapotranspiration are calculated for the time period from 1961-2013.

This dataset may be highly valuable for users in the field of hydrology, agriculture, ecology etc. as it aims to provide ET0 in a high spatial resolution and a long time period. Data for calculating ET0 by recommended PM is usually not available for such long time spans and/or with this spatial and temporal resolution. However, the method presented in this study tries to combine both strengths of long time series, high spatial and temporal resolution provided by the temperature based HM and the physical more realistic radiation based PM by adjusting HM.

Acknowledgements

The authors want to thank the Federal Ministry of Science, Research and Economy (Grant 1410K214014B) for financial support. We also like to thank Johann Hiebl for providing the SPARTACUS data and for fruitful discussions on the manuscript. The Austrian Weather Service (ZAMG) is acknowledged for providing the data of 42 meteorological stations. We would also like to thank two anonymous reviewers for the valuable comments which improved the manuscript substantially.

References

Aguila, C., and Polo, M. J.: Generating reference evapotranspiration surfaces from the Hargreaves equation at watershed scale, Hydrol. Earth Syst. Sci., 15, 2495–2508, 2011.

Allen, R. G., Pereira, L. S., Raes, D., and Smith, M.: Crop evapotranspiration – Guidelines for computing crop water requirements, FAO Irrigation and drainage paper 56, Rome, 15 pp, 1998.

Bautista, F., Bautista, D., and Delgado-Carranza, C.: Calibrating the equations of Hargreaves and Thornthwaite to estimate the potential evapotranspiration in semi-arid and subhumid tropical climates for regional applications, Atmósfera 22(4), 331-348, 2009.

Bindi, M., and Miglietta, F.: Estimating daily global radiation from air temperature and rainfall measurements, Clim. Change, 1, 117-124, 1991.

Bormann, H.: Sensitivity analysis of 18 different potential evapotranspiration models to observed climatic change at German climate stations, Clim. Ch., 104, 729-753, 2011.

Bristow, K. L., and Campbell, G. S.: On the relationship between incoming solar radiation and daily maximum and minimum temperature, Agric. Forest. Meteorol., 31(2), 159-166, 1984.Chattopadhyay N. and Hulme M.: Evaporation and potential evapotranspiration in India under conditions of recent and future climate changes, Agric. Forest. Meteorol. 87, 55-74, 1997.

Doorenbros, J., and Pruitt, O. W.: Crop water requirements. FAO Irrigation and Drainage Paper 24, Rome, 144 pp, 1977.

Farr, T.G., Kobrick, M.: Shuttle Radar Topography Mission produces a wealth of data, Amer. Geophys. Union Eos, 81, 583-585, 2000.

Gavilán, P., Lorite, I. J., Tornero, S., and Berengena, J.: Regional calibration of Hargreaves equation for estimating reference ET in a semiarid environment, Agr. Water Manage., 81, 257-281, 2006.

Hargreaves, G. H., and Allen, R.: History and Evaluation of Hargreaves Evapotranspiration Equation, J. Irrig. Drain Eng., 129(1), 53-63, 2003.

Hargreaves, G. H., and Samani, Z. A.: Estimating potential evapotranspiration, J. Irrig. Drain Eng., 108(3), 225-230, 1982.

Hargreaves, G. H., and Samani, Z. A.: Reference crop evapotranspiration from temperature, Appl. Eng. Agric., 1, 96-99, 1985.

Hargreaves, G. H.: Moisture Availability and Crop Production, Trans. ASABE, 18 (5): 980-984, 1975.

Hargreaves, G. L., Hargreaves, G. H., and Riley, J. P.: Irrigation water requirements for Senegal River Basin, J. Irrig. Drain. Eng., 111(3), 265-275, 1985.

Hiebl, J., and Frei, C.: Daily temperature grids for Austria since 1961 – concept, creation and applicability, submitted to Theor. Appl. Climatol.

Lhomme, J.-P.: Towards a rational definition of potential evapotranspiration, Hydrol. Earth Sys. Sci., 1(2), 257-264, 1997.

Mancosu, N., Snyder, R. L., and Spano, D.: Procedures to Develop a Standardized Reference Evapotranspiration Zone Map, J. Irrig. Drain Eng., 140, A4014004, 2014.

Makowski, K., Jaeger E. B., Chiacchio, M., Wild, M., Ewen, T., and Ohmura, A.: On the relationship between diurnal temperature range and surface solar radiation in Europe, J. Geophys. Res., 114, D00D07, 2009.

McMahon, T. A., Peel, M. C., Lowe, L., Srikanthan, R., and McVicar, T. R.: Estimating actual, potential, reference crop and pan evaporation using standard meteorological data: a pragmatic synthesis, Hydrol. Earth Sys. Sci., 17, 1331–1363, 2013.

McVicar, T. R., Van Niel, T. G., Li, L., Hutchinson, M. F., Mu, X.-M., and Liu, Z.-H.: Spatially distributing monthly reference evapotranspiration and pan evaporation considering topographic influences, J. Hyd., 338, 196-220, 2007.

Pan, T., Wu, S., Dai, E., and Liu, Y.: Estimating the daily global solar radiation spatial distribution from diurnal temperature ranges over the Tibetan Plateau in China, Ap. Energy, 107, 384-393, 2013.

Pandey, V., Pandey, P. K., and Mahanta, A. P.: Calibration and performance verification of Hargreaves Samani equation in a humid region, Irrig. and Drain., 63, 659–667, 2014.

Samani, Z.: Estimating Solar Radiation and Evapotranspiration Using Minimum Climatological Data (Hargreaves-Samani equation), J. Irr. Drain. Eng., 126 (4), 265-267, 2000.

Shelton, M. L.: Hydroclimatology, Cambridge University Press, Cambridge, United Kingdom, 2009.

Tabari, H. and Talaee, P.: Local Calibration of the Hargreaves and Priestley-Taylor Equations for Estimating Reference Evapotranspiration in Arid and Cold Climates of Iran Based on the Penman-Monteith Model, J. Hydrol. Eng., 16(10), 837-845, 2011.

Tegos, A., Malamos, M., and Koutsoyiannis, D.: A parsimonious regional parametric evapotranspiration model based on a simplification of the Penman–Monteith formula, J. Hyd., 524, 708-714, 2015.

Todorovic, M., Karic, B., and Pereira, L. S.: Reference evapotranspiration estimate with limited weather data across a range of Mediterranean climates, J. Hyd., 481, 166-176, 2011.

Xu, C.-Y., and Chen D.: Comparison of seven models for estimation of evapotranspiration and groundwater recharge using lysimeter measurement data in Germany, Hydrol. Processes, 19, 3717-3734, 2005.

Xu, C.-Y., and Singh, V. P.: Evaluation and generalization of radiation-based equations for calculating evaporation, Hydrol. Processes, 14, 339-349, 2000.

Xu, C.-Y., and Singh, V. P.: Evaluation and generalization of temperature-based equations for calculating evaporation, Hydrol. Processes, 14, 339-349, 2001.

Table 1. Location, altitude and setting of the 42 meteorological stations used for calibration.

	Station	Lon (°)	Lat (°)	Alt (m)	Setting
1	Aflenz	15.24	47.55	783	Mountainous
2	Alberschwende	9.85	47.46	715	Mountainous
3	Arriach	13.85	46.73	870	Mountainous
4	Bregenz	9.75	47.50	424	Lakeside
5	Dornbirn	9.73	47.43	407	Valley
6	Feldkirchen	14.10	46.72	546	Valley
7	Feuerkogel	13.72	47.82	1618	Summit
8	Fischbach	15.64	47.44	1034	Mountainous
9	Galzig	10.23	47.13	2084	Alpine
10	Graz_Universitaet	15.45	47.08	366	City
11	Grossenzersdorf	16.56	48.20	154	Lowland
12	Gumpoldskirchen	16.28	48.04	219	Lowland
13	Irdning_Gumpenstein	14.10	47.50	702	Valley
14	Ischgl_Idalpe	10.32	46.98	2323	Alpine
15	Jenbach	11.76	47.39	530	Valley
16	Kanzelhoehe	13.90	46.68	1520	Summit
17	Krems	15.62	48.42	203	Lowland
18	Kremsmünster	14.13	48.06	382	Lowland
19	Langenlois	15.70	48.47	207	Lowland
20	Lilienfeld_Tarschberg	15.59	48.03	696	Mountainous
21	Lofereralm	12.65	47.60	1624	Alpine
22	Lunz_am_See	15.07	47.85	612	Valley
23	Lutzmannsburg	16.65	47.47	201	Lowland

24	Mariapfar	13.75	47.15	1153	Mountainous
25	Mariazell	15.30	47.79	864	Mountainous
26	Neumarkt	14.42	47.07	869	Mountainous
27	Patscherkofel	11.46	47.21	2247	Summit
28	Poertschach	14.17	46.63	450	Lakeside
29	Retz	15.94	48.76	320	Lowland
30	Reutte	10.72	47.49	842	Valley
31	Rudolfshuette-Alpinzentrum	12.63	47.13	2304	Alpine
32	Schaerding	13.43	48.46	307	Lowland
33	Schmittenhoehe	12.74	47.33	1973	Alpine
34	Sonnblick	15.96	47.05	3109	Summit
35	Spittal_Drau	13.49	46.79	542	Valley
36	Villacheralpe	13.68	46.60	2156	Summit
37	Virgen	12.46	47.00	1212	Valley
38	Weissensee_Gatschach	13.29	46.72	945	Lakeside
39	Wien_Donaufeld	16.43	48.26	161	City
40	Wien_Hohewarte	16.36	48.25	198	City
41	Wien_Unterlaa	16.42	48.12	201	City
42	Wolfsegg	13.67	48.11	638	Lowland

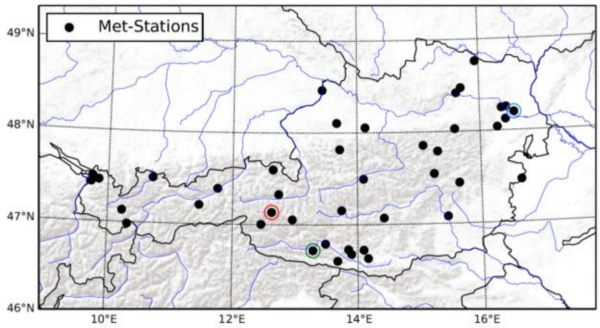

Figure 1. Location of the meteorological stations used for calibration; coloured circles around points indicate stations that are exemplary displayed in other plots: Grossenzersdorf (blue), Weissensee_Gatschach (green) and Rudolfshuette-Alpinzentrum (red).

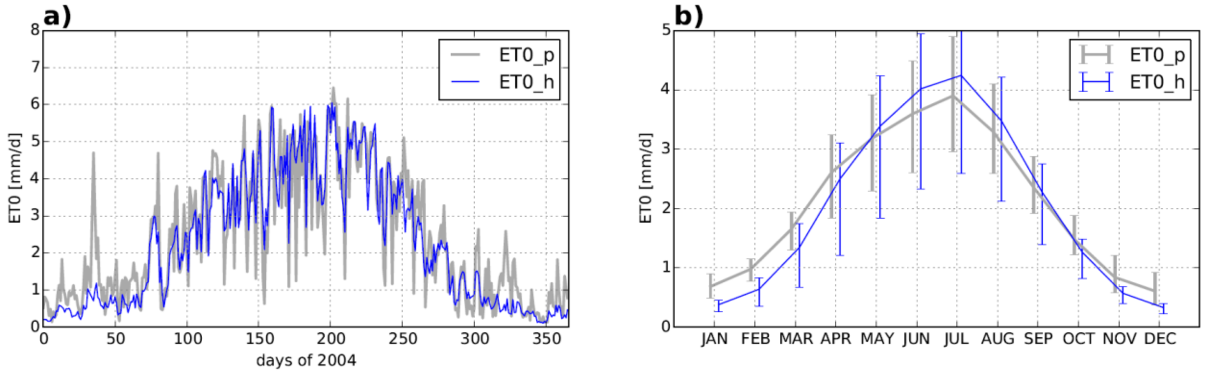

Figure 2. Daily time series of ET0 in 2004 for ET0 based on PM (ET0_p) and HM (ET0_h) at the station Grossenzersdorf (a); Monthly mean ET0 from 2004 to 2013 averaged over all station, error bars denote for the spread among all stations (b).

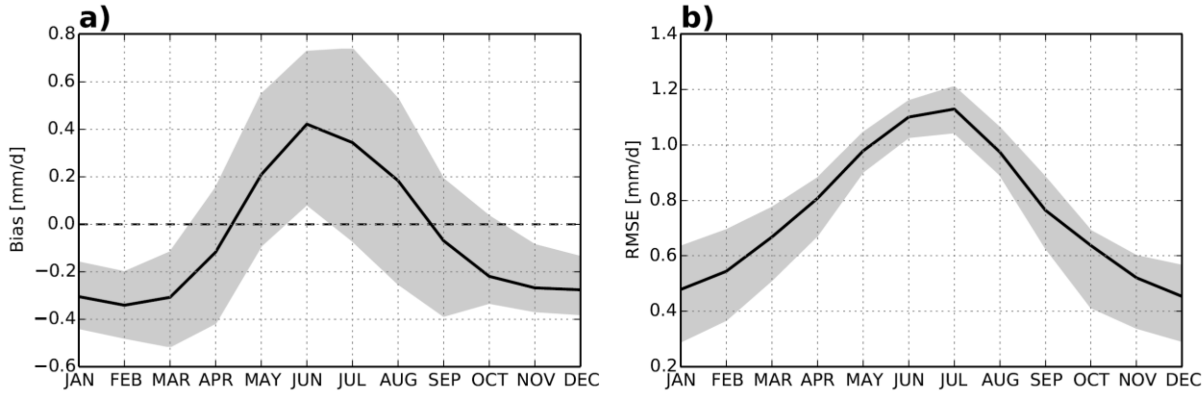

Figure 3. Monthly Bias (a) and monthly Root Mean Square Error (b) between daily ET0_p and ET0_h for all stations; the grey shading indicates the spread among the different stations.

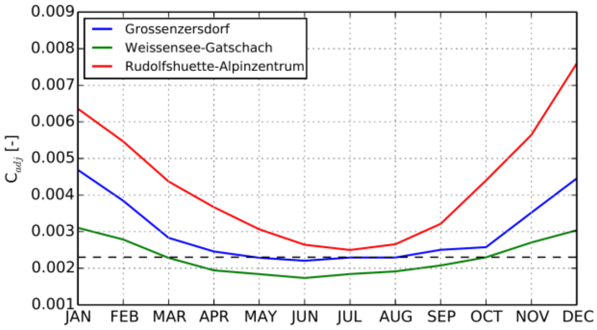

Figure 4. Monthly values of C_{adj} at three different stations, the dashed black lines indicates the original C value of 0.0023 from Hargreaves et al. (1985).

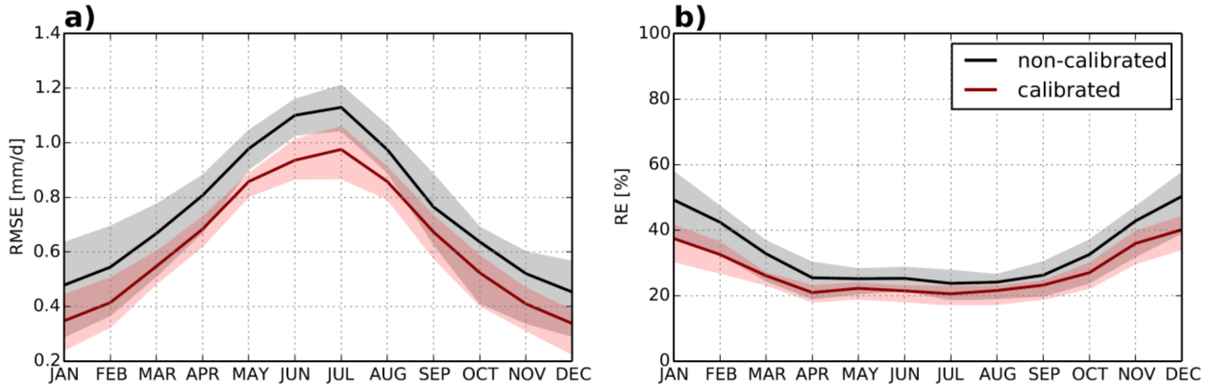

Figure 5. Monthly Root Mean Square Error (a) and monthly Relative Error (b) between daily ET0_p and ET0_h (black) and ET0_p and ET0_h.c (red).

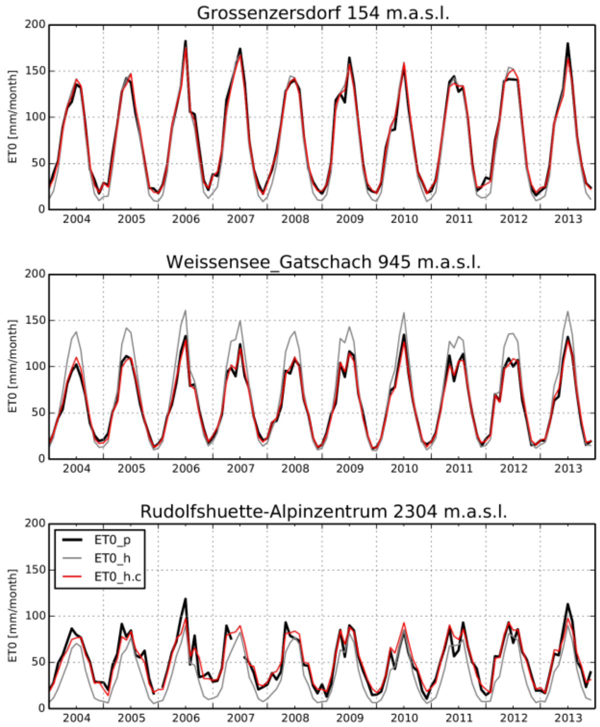

Figure 6. Monthly ET0 sums derived from ET0_p, ET0_h and ET0_h.c for three stations located at different altitudes.

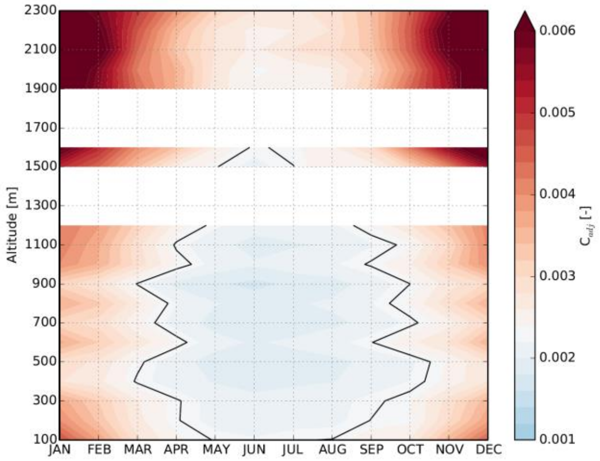

Figure 7. Monthly variations of C_{adj} with respect to altitude; the black contour line defines the original Hargreaves Calibration Parameter C value of 0.0023; stations are binned to classes of altitude from 100 to 2300 m every 100 m; white areas denote classes of altitude with no station available.

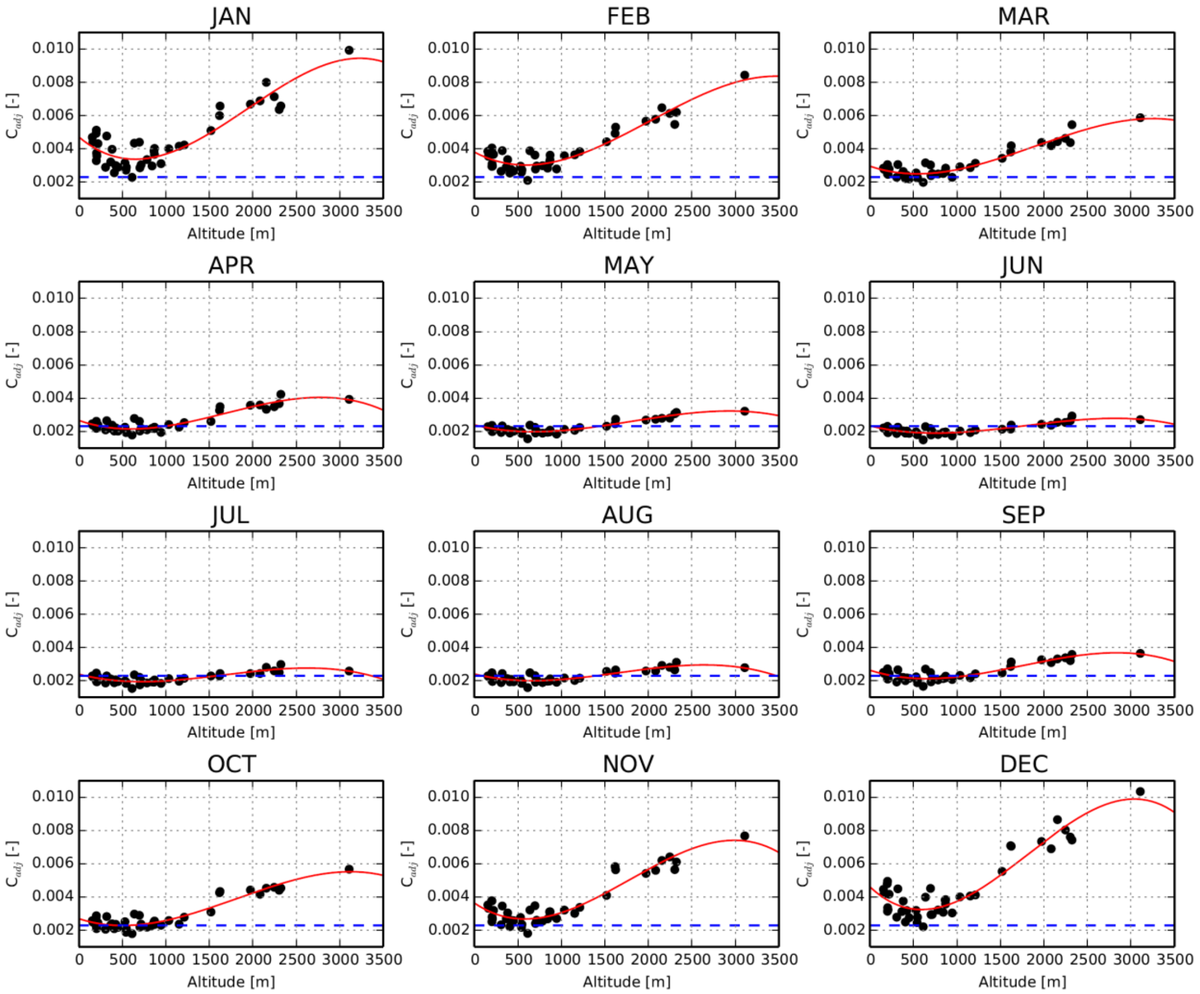

Figure 8. Station-wise monthly third-order polynomial fit of the Hargreaves Calibration Parameter C_{adj} against altitude; the blue dotted line indicates the original C value of 0.0023.

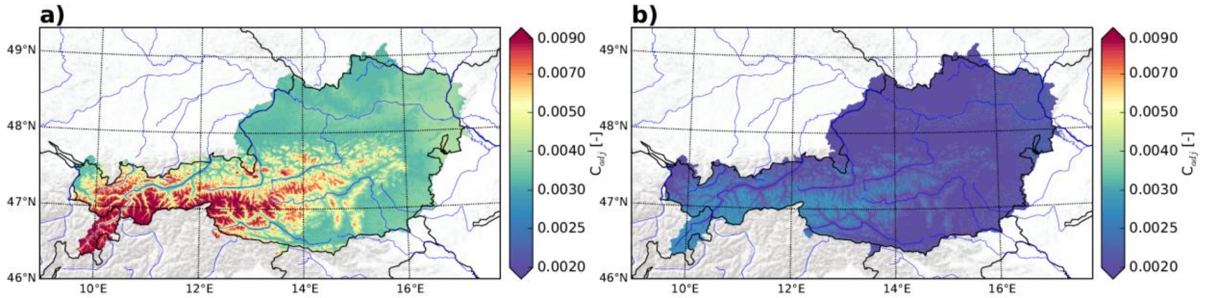

Figure 9. Spatially interpolated C_{adj} values for January 1st (a) and July 1st (b).

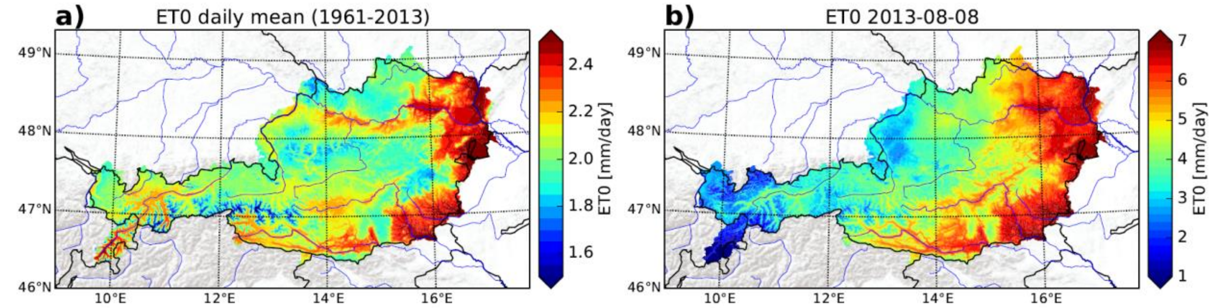

Figure 10. Climatological daily mean ET0 from 1961-2013 (a); example of a daily field of ET0 on August 8th 2013 (b).

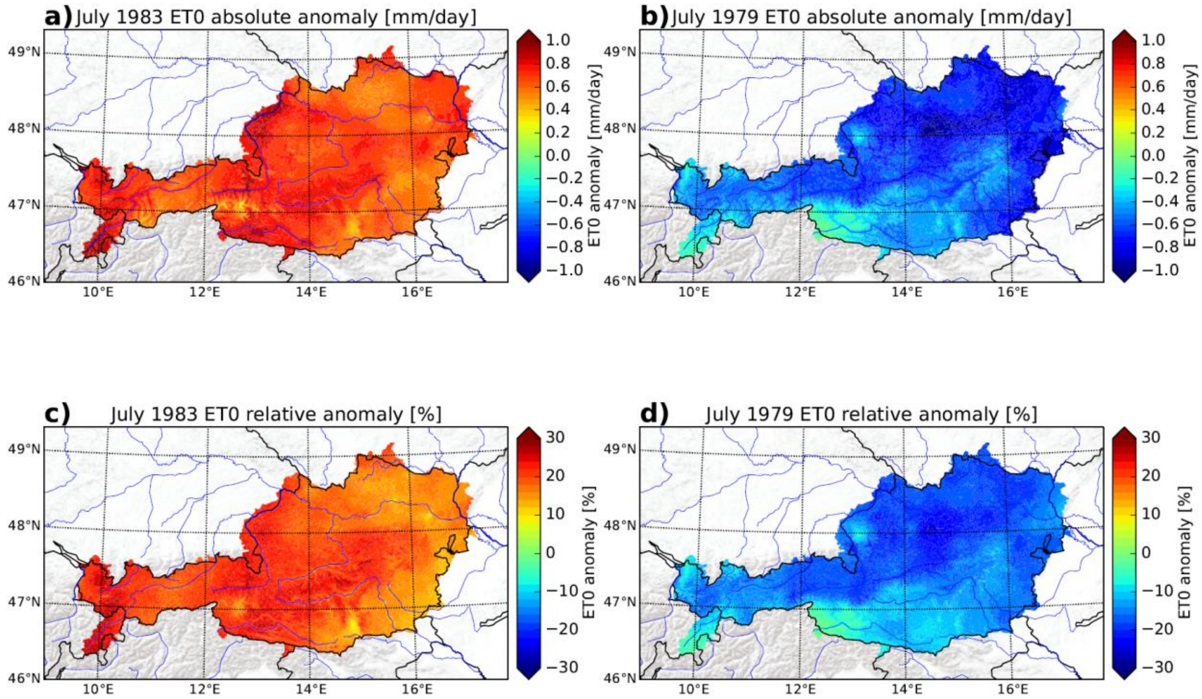

Figure 11. Upper panel: absolute anomalies of ET0 sum in July 1983 (a) and July 1979 (b) with respect to the climatological mean in July from 1961-2013; lower panel: corresponding relative anomaly (c, d).

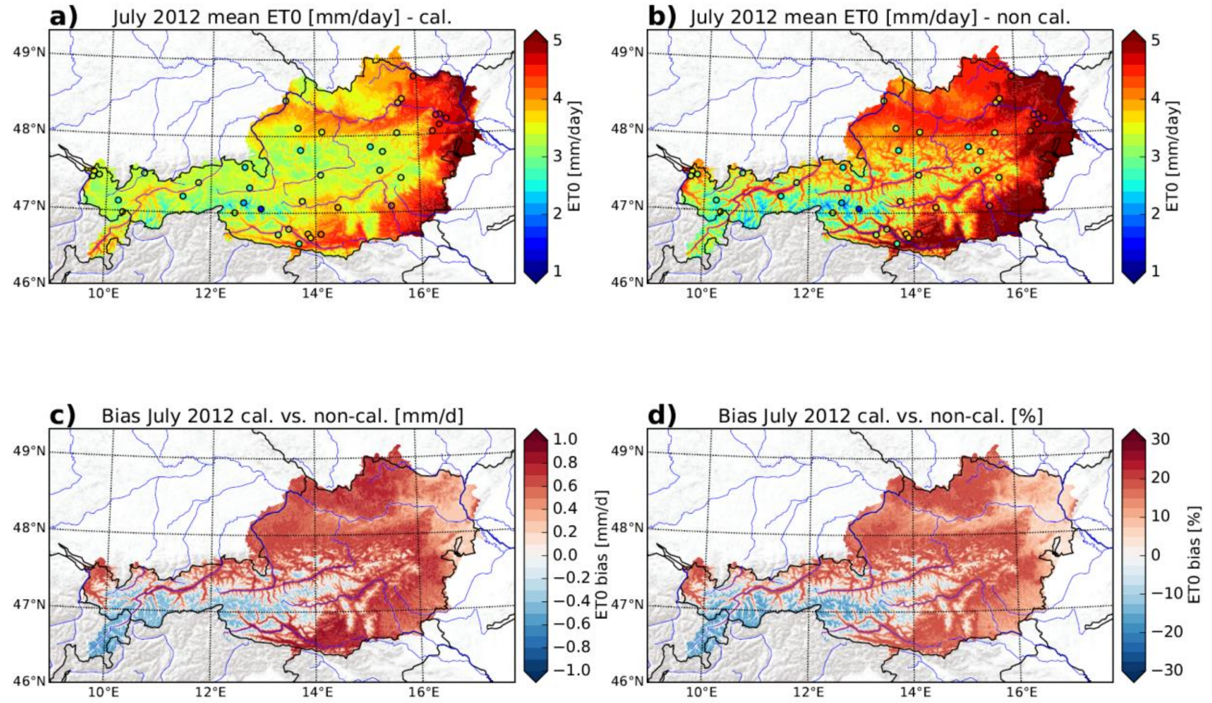

Figure 12. July 2012 monthly mean ET0 based on C_{adj} values – ET0_h.c (a), using the original C of 0.0023 for the whole grid ET0_h (b) and the corresponding absolute (c) and relative bias (d); the dots in (a) and (b) denote for the PM ET0 at the stations.

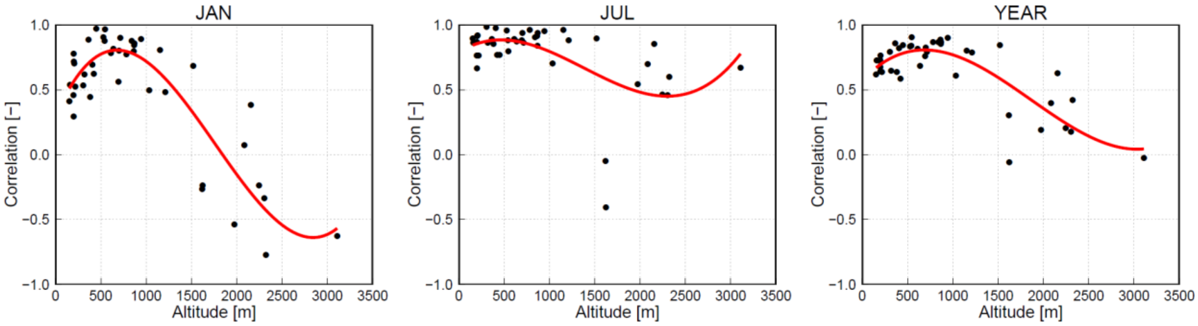

Figure 13. Station-wise Correlation of Global Radiation and Diurnal Temperature Range (T_{max}-T_{min}) against altitude represented by black dots in January (left), July (middle) and all-year (right); the red line represents a third-order polynomial fit.

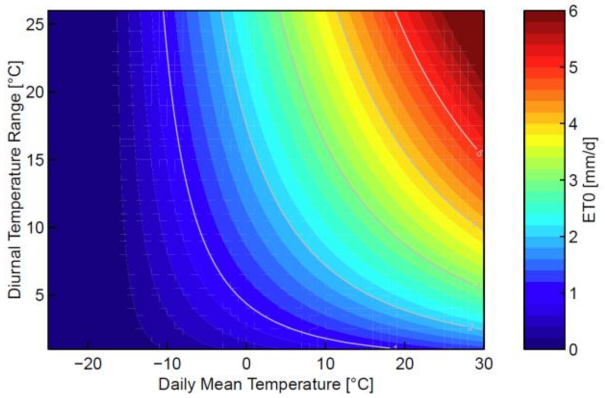

Figure 14. ET0 response to varying Daily Mean Temperature and Diurnal Temperature Range; ET0 values are calculated with 1st of April Top of the Atmosphere Radiation and the original C value of 0.0023.

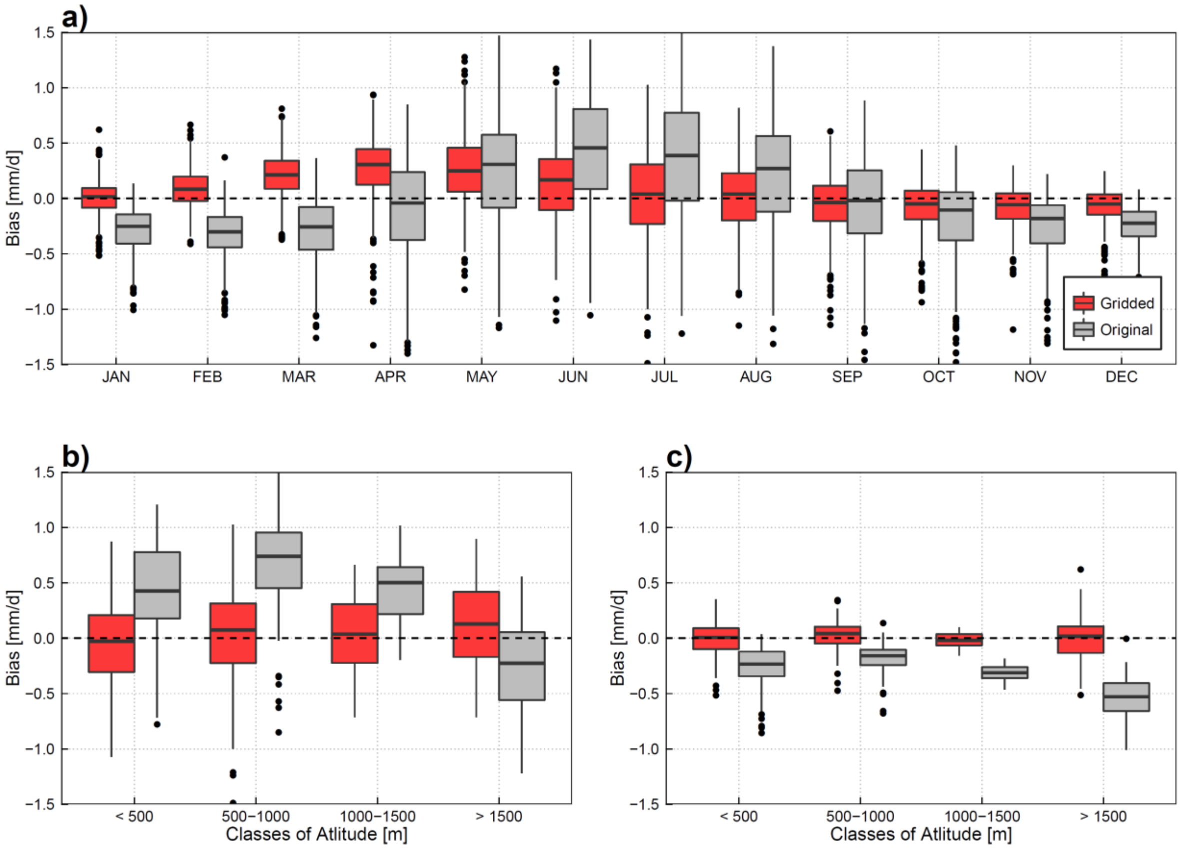

Figure 15. Boxplots of monthly mean bias of the station-wise original Hargreaves ET0 (grey) and the final gridded, re-calibrated ET0 (red) against Penman-Monteith ET0 (a); stratified by different classes of altitude in July (b) and January (c);